Real-Time Magnetic Field Calibration Method Based on Extended Kalman Filter

Real-Time Magnetic Field Calibration Method Based on Extended Kalman Filter

LI Wenkuan[1,2], CAI Haoyuan[*1], ZHAO Shenglin[1,2] and LIU Chunxiu[1]

[1]Aerospace Information Research Institute, Chinese Academy of Science, Beijing, China
[2]University of Chinese Academy of Sciences, Beijing, China

E-mail: hycai@mail.ie.ac.cn

Abstract. VINS makes roll and pitch observable because IMU is added, but if yaw also needs to be observable, the magnetometer needs to be used. But it is highly susceptible to interference from surrounding ferromagnetic materials. This paper first improves the traditional complementary filtering to eliminate the influence of linear acceleration during motion, then uses it fuses the accelerometer and gyroscope data to make more accurate prediction of the magnetometer data, and an Extended Kalman Filtering is used to implement magnetometer calibration. In the convenience experiment, our algorithm reduces the error RMS from 71.12uT to 11.77uT, while the ellipsoid fitting can't calibrate correctly. In the calibration speed and accuracy experiment, our algorithm can realize the maximum value of the error distance after 5s is 0.42uT, which is better than the 0.98uT of the gyro-only compensation. In the stability experiment, within 10 minutes, the data calibrated by our algorithm drift only 4.12uT, which is better than 11.10uT of the gyro-only compensation. Finally, a convenient, accurate and stable real-time magnetometer calibration algorithm is realized. It has a wide range of functions in consumer electronics, VINS and military.

1. Introduction

Compared with visual SLAM, VINS (Visual-Inertial Navigation System) is added with IMU, which makes roll and pitch observable, but yaw is still unobservable. To get an absolutely observable yaw, a magnetometer is usually used. The main way to determine the yaw is obtained by measuring the earth's magnetic field by a magnetometer[1][2][3]. However, the error of the instrument and the interference of the environment are two important factors affecting the accuracy of the magnetic yaw. The error caused by the environmental magnetic field is the most difficult to control and compensate[4][5], so it is often necessary to calibrate the magnetometer data.

The methods of calibration are mainly divided into two categories, one is static calibration before the instrument is used, it relies on auxiliary equipment and is costly and complicated, so it is generally only used for high-end equipment[6]. and the other is dynamic calibration when the instrument is used[7].The dynamic calibration method can be divided into two types depending on whether it requires an external device. One is to model the magnetic field and use only the magnetometer to calculate the calibration parameters based on the constraints of the geomagnetic field[8][9]. The most common methods are the ellipsoid fitting method and the maximum and minimum method. [10] used the Newton iterative method to linearize the ellipsoid surface equation, and then calculate by least squares method and total least squares method respectively. Although this method can achieve good

results, it has strict requirements on data, so it is often necessary to perform certain operations (such as around "8") to collect data, which is difficult to achieve in many applications of VINS (such as UAV, robot), not only that, it needs to be calibrated again after the usage environment changes, it cannot run in real time. Another method is to use an external device, the most commonly used is the Inertial Measurement Unit (IMU). [11] formulates data as the solution to a maximum likelihood problem and the calculate offline. The algorithm is shown to give good results using data from two different commercially sensors. Although it achieves more convenient calibration, but it cannot work in real time. [12] achieved a real-time calibration using EKF (Extended Kalman Filter), it fusions data of magnetometer and gyroscope, but due to gyroscope's drift, the error increases with time.

This paper first improves the traditional complementary filtering to eliminate the influence of linear acceleration during motion, then uses it fuses the accelerometer and gyroscope data to make more accurate prediction of the magnetometer data, and then an Extended Kalman Filtering are used to implement magnetometer calibration. Our algorithm enables stable, convenient, highly accurate and real-time magnetometer calibration.

2. Magnetic measurement model

2.1. Magnetic field model

In the absence of any interference or error, [13] gives the relationship between the magnetometer data $\mathbf{B}_c$ and the local geomagnetic vector $\mathbf{B}_e$:

$$\mathbf{B}_c = \mathbf{R}\mathbf{B}_e \tag{1}$$

Where $\mathbf{R}$ is the rotation matrix of the magnetometer. However, in general, the measurement is affected by magnetic field interference,[14] gives the relationship:

$$\mathbf{B}_p = \mathbf{W}\mathbf{R}\mathbf{B}_e + \mathbf{V} \tag{2}$$

Where $\mathbf{B}_p$ is the actual measurement of the magnetometer, which is affected by magnetic field interference. $\mathbf{W}$ is a soft iron interference, which is a 3×3 matrix. $\mathbf{V}$ is a hard iron interference, which is a 3×1 vector. The calibration model of the magnetometer after inversion is:

$$\mathbf{B}_c = \mathbf{W}^{-1}(\mathbf{B}_p - \mathbf{V}) \tag{3}$$

When the surrounding environment is constant, $\mathbf{W}$ and $\mathbf{V}$ are usually considered to be a fixed value. However, in the daily use of VINS such as mobile robot, the surrounding environment is always changing. So, the soft and hard iron interference will undergo a large change. This means that the magnetometer needs real-time dynamic calibration during the use of daily life.

2.2. Magnetic field measurement track

From equation (1), we can know that the calibrated magnetometer data should locate on the surface of the sphere:

$$(\mathbf{B}_c)^T\mathbf{B}_c = (\mathbf{R}\mathbf{B}_e)^T\mathbf{R}\mathbf{B}_e = \mathbf{B}_e{}^T\mathbf{R}^T\mathbf{R}\mathbf{B}_e = B^2 \tag{4}$$

Where B is the local geomagnetic field strength, $B = \mathbf{B}_e{}^T\mathbf{B}_e$. The sphere canter is origin, and the radius is equal to the local geomagnetic field strength B. When disturbed, equation (4) will be :

$$[\mathbf{W}^{-1}(\mathbf{B}_p - \mathbf{V})]^T[\mathbf{W}^{-1}(\mathbf{B}_p - \mathbf{V})] = (\mathbf{B}_p - \mathbf{V})^T(\mathbf{W}^{-1})^T\mathbf{W}^{-1}(\mathbf{B}_p - \mathbf{V}) = B^2 \tag{5}$$

The uncalibrated magnetometer measurement should locate on the surface of the ellipsoid, the centre of the ellipsoid is (V_x, V_y, V_z),and the shape of the ellipsoid is determined by the matrix $(\mathbf{W}^{-1})^T\mathbf{W}^{-1}$.

3. Improved complementary filtering and magnetic field data recursion

The IMU is a device that measures the angular velocity and acceleration of an object's three axes. The accelerometer is sensitive to disturbances such as vibration, but the attitude calculated by long-term data is credible; the gyroscope is not sensitive to vibration, but the long-term use of the gyroscope will drift. There are already many researchers working on IMU data fusion[15].

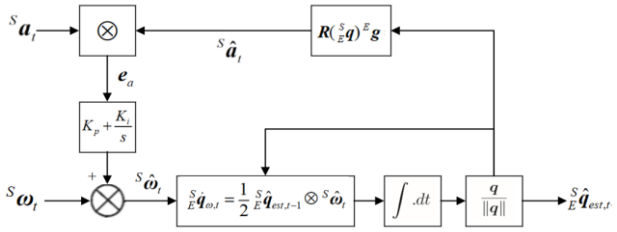

Figure 1. The complementary filtering proposed by Mahony

In Figure 1, $\boldsymbol{a}_t$ and $\boldsymbol{\omega}_t$ represent the acceleration and angular velocity at time t, quaternion $\mathbf{q}$ and rotation matrix $\mathbf{R}$ are used to represent attitude, K_p and K_i are error compensation parameters, and superscript S and E represent sensor and earth coordinate respectively.

The algorithm estimates the acceleration $\widehat{\boldsymbol{a}}_t$ at time t by rotating the gravitational acceleration, and then use it to calculate the error:

$$\boldsymbol{e}_a = \boldsymbol{a}_t \times \widehat{\boldsymbol{a}}_t \tag{6}$$

And accumulate the $\boldsymbol{e}_a$ to get the integral feedback error $\boldsymbol{e}'_a$ then subtracts them from the gyroscope measurement $\boldsymbol{\omega}_t$to obtain $\widehat{\boldsymbol{\omega}}_t$, Then use it to update the quaternion to get the attitude at this time.:

$$\widehat{\boldsymbol{\omega}}_t = \boldsymbol{\omega}_t + (\mathrm{K}_p \boldsymbol{e}_a + \mathrm{K}_i \boldsymbol{e}'_a) \tag{7}$$

The K_p and K_i in the complementary filtering are set to 1 and 0, but in this case, the result is affected by the linear acceleration, so the K_p is improved in this paper:

$$\mathrm{K}_p = \exp(-2 \times \left\| 1 - \|\boldsymbol{a}_t\| \right\|) \tag{8}$$

Where$\mathbf{B}_{\mathrm{c,k}}$ and $\mathbf{B}_{\mathrm{c,k+1}}$ are magnetic field data at time k and time k+1, respectively.

$$\mathbf{B}_{\mathrm{c,k+1}} = \Delta\mathbf{R}_{\mathrm{k}} \mathbf{B}_{\mathrm{c,k}} \tag{10}$$

Where $\Delta\mathbf{R}_{\mathrm{k}} = \mathbf{R}_{\mathrm{k+1}} {\mathbf{R}_{\mathrm{k}}}^{\mathrm{T}}$, If the magnetometer and the IMU are on the same carrier, the attitude changes perceived by the two sensors should be the same. $\Delta\mathbf{R}_{\mathrm{k}}$ can be calculated by the IMU data through the improved complementary filtering. This equation can obtain the magnetometer data at this moment from the previous moment recursively combined with the IMU data.

4. IMU-compensated real-time EKF magnetic field calibration

4.1. Establish a state equation

There are 12 values that need to be updated, which includes the three values of magnetic field data $\mathbf{B}_{\mathrm{c,k}} = (\mathrm{B}_{\mathrm{c,x}}, \mathrm{B}_{\mathrm{c,y}}, \mathrm{B}_{\mathrm{c,z}})^{\mathrm{T}}$, the three values of the hard iron interference vector $\mathbf{V}_{\mathrm{k}} = (\mathrm{V}_{\mathrm{x}}, \mathrm{V}_{\mathrm{y}}, \mathrm{V}_{\mathrm{z}})^{\mathrm{T}}$, and because the soft iron interference matrix is symmetrical, only six of the nine elements in the matrix are required, $\mathbf{W}_{\mathrm{element,k}}$=($\mathrm{W}_{11}$, W_{22}, W_{33}, W_{12}, W_{13}, W_{23}). The state variable can be written as:

$$\mathbf{X}_{\mathrm{k}} = \left[\mathbf{B}_{\mathrm{c,k}}^{\mathrm{T}}, \mathbf{W}_{\mathrm{element,k}}, \mathbf{V}_{\mathrm{k}}^{\mathrm{T}}\right]^{\mathrm{T}} \tag{11}$$

Therefore, the state equation $\widehat{\mathbf{X}}_{\mathrm{k/k\text{-}1}} = \mathbf{f}(\widehat{\mathbf{X}}_{\mathrm{k\text{-}1}})$ in the Kalman Filter can be written as:

$$\mathbf{B}_{\mathrm{c,k}} = \Delta\mathbf{R}\mathbf{B}_{\mathrm{c,k-1}} \tag{12a}$$

$$\mathbf{W}_{\mathrm{element,k}} = \mathbf{W}_{\mathrm{element,k\text{-}1}} \tag{12b}$$

$$\mathbf{V}_{\mathrm{k}} = \mathbf{V}_{\mathrm{k-1}} \tag{12c}$$

According to the formula of the variance matrix $\mathbf{Q}_{\mathrm{w}} = \mathrm{E}[\mathbf{w}\mathbf{w}^{\mathrm{T}}]$ (where $\mathbf{w}$ is the state transition noise sequence), the variance matrix of the state transition is calculated as:

$$\mathbf{Q}_{k-1} = \begin{bmatrix} \mathbf{B}_{c,k-1}\mathbf{B}_{c,k-1}^{T}\boldsymbol{\sigma}_{\Delta\mathbf{R}}^{2}\Delta t^{2} & \mathbf{0}_{3*9} \\ \mathbf{0}_{9*3} & \mathbf{0}_{9*9} \end{bmatrix} \tag{13}$$

Where $\boldsymbol{\sigma}_{\Delta\mathbf{R}}^{2}$ is a covariance matrix of $\Delta\mathbf{R}$. we will collect static data to estimate this matrix.

The state equation function **f** is a linear equation, it is easy to write in a linear form, and its Jacobian matrix is:

$$\mathbf{F}_{k-1} = \begin{bmatrix} \Delta\mathbf{R} & \mathbf{0}_{3*9} \\ \mathbf{0}_{9*3} & \mathbf{I}_{9*9} \end{bmatrix} \tag{14}$$

4.2. Establishing a measurement equation

Taking the actual measured data of the magnetometer as the measured value in the EKF, then the measurement equation $\mathbf{Z}_k = \mathbf{h}(\mathbf{X}_k) + \mathbf{V}_k$ can be written as:

$$\mathbf{B}_{p,k} = \mathbf{W}_k\mathbf{B}_{c,k} + \mathbf{V}_k + \boldsymbol{\varepsilon}_m \tag{15}$$

Where $\mathbf{B}_{p,k}$ is the uncalibrated magnetometer data at time k. $\mathbf{W}_k$ and $\mathbf{V}_k$ are the soft iron interference at time k. $\boldsymbol{\varepsilon}_m$ is the measurement noise of the magnetometer. And its Jacobian matrix is:

$$\mathbf{H}_k = \left[\mathbf{W}_{k|k-1}\middle|\begin{matrix} x_{k|k-1,1} & 0 & 0 & x_{k|k-1,2} & x_{k|k-1,3} & 0 \\ 0 & x_{k|k-1,2} & 0 & x_{k|k-1,1} & 0 & x_{k|k-1,3} \\ 0 & 0 & x_{k|k-1,3} & 0 & x_{k|k-1,1} & x_{k|k-1,2} \end{matrix}\middle|\mathbf{I}_{3\times3}\right] \tag{16}$$

In addition, according to the formula of the variance matrix $\mathbf{R}_w = E[\mathbf{v}\mathbf{v}^T]$ (where **v** is the measurement noise sequence), the variance matrix in the measurement process is:

$$\mathbf{R}_k = \sigma_m^2\mathbf{I}_{3\times3} \tag{17}$$

Where σ_m^2 is the variance of the magnetometer noise $\boldsymbol{\varepsilon}_m$. For different devices, we will collect static data to estimate this value.

5. Data collection and comparison method

In this paper, we use LMPS-B2 which is a 9-axis AHRS(Attitude and Heading Reference System) produced by ALUBI to collect the magnetometer, accelerometer and gyroscope data, the sampling frequency is 100Hz. We collected 10 minutes of static data to estimate the σ_m and $\boldsymbol{\sigma}_{\Delta\mathbf{R}}^{2}$, and the results are: $\sigma_m^2 = 0.7$, $\boldsymbol{\sigma}_{\Delta\mathbf{R}}^{2} = \begin{bmatrix} 1.2*10^{-8} & 3.0*10^{-3} & 1.4*10^{-3} \\ 3.0*10^{-3} & 4.0*10^{-8} & 2.5*10^{-3} \\ 1.4*10^{-3} & 2.5*10^{-3} & 6.5*10^{-8} \end{bmatrix}$.

In order to better compare the calibration results, we make the following provisions:

- Environment: Under the same experiment, the external environment remains unchanged.
- Raw magnetic field (*mag-raw*): rotates the unit several times around "8", collecting IMU data and magnetic field distributed in each quadrant.
- Calibrated magnetic field: (*mag-cal-xxx*): collect the data under different experimental conditions, input these data into different algorithms to get the parameters W and V, then use the parameters to calibrate *mag-raw* to get *mag-cal-elli*, *mag-cal-gyro* and *mag-cal-our*.
- Ideal magnetic sphere (*sphere-ideal*): use the origin as the centre of the sphere and B as the radius to make the ideal magnetic sphere.

At the same time, in order to more clearly compare the experimental results. This paper uses error distance between a magnetic field data point to the surface of *sphere-ideal*:

$$D = \left|\sqrt{\left(B_{c,x}\right)^2 + \left(B_{c,y}\right)^2 + \left(B_{c,z}\right)^2} - B\right| \tag{18}$$

Where B represents the magnetic field strength of *sphere-ideal*. Then, calculate the mean of all D:

$$M = \frac{1}{n}\sum_{i=1}^{n} D_i \tag{19}$$

The smaller value of M, representing the closer distance between the magnetic field data and the ideal sphere, that is, the calibration effect is better.

6. Comparison experiment

In this paper, we compare the calibration effect of the ellipsoid fitting, the gyro-only compensation algorithm and our algorithm. The experiment is divided into three aspects: convenience experiment, accuracy and speed experiment and stability experiment.

6.1. Convenience experiment

The purpose of this experiment is to test the convenience of our algorithm. Firstly, the LMPS-B2 is fully rotated (around "8") to acquire the *mag-raw*, so that the data satisfies the requirements of the ellipsoid fitting. All data is then input into the ellipsoid fitting to calculate calibration parameters and *sphere-ideal*.

Then, LMPS-B2 is moved to collect data simulating the mobile phone's activity in daily use, such as walking around with the phone, answering the phone, shaking the phone.

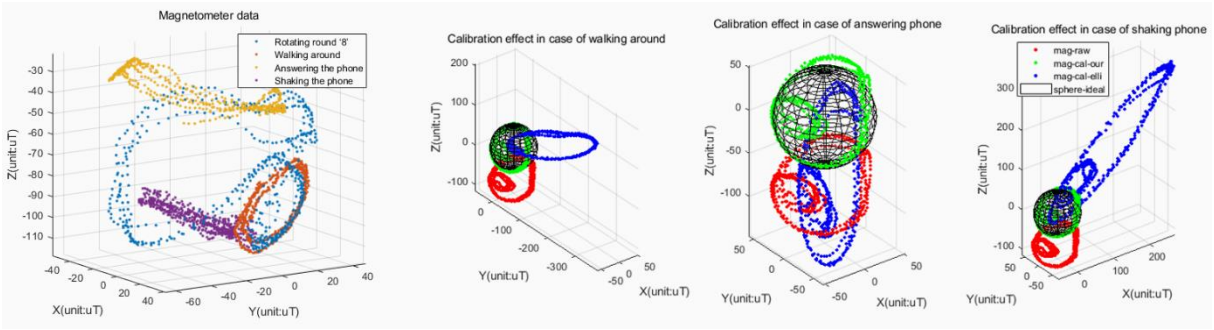

Figure 2. Magnetometer data and the calibration effect in three cases

The left picture in Figure 2 shows the measurement of the magnetometer in four cases. It can be found that when rotating around "8", the measurement is widely distributed, and the data meet the requirements of the ellipsoid fitting. However, in the other three cases, because the activity is simple and the measurement distribution is concentrated. Then input these data collected in the other three cases into our algorithm and ellipsoid fitting to calculate the magnetic interference parameters.

Table 1. Calibration result in the case of answering phone

	mag-raw	*mag-cal-our*	*mag-cal-elli*
W_{11}	0.9937	0.9699	1.3247
V_2	-9.6965uT	-8.7133uT	-1.0486uT
B	52.5824uT	53.0481uT	84.6368uT
RMS	71.1165uT	11.7660uT	68.4142uT

As shown in table 1, when doing the motion of answering phone, because the measurement distribution is not extensive enough, the ellipsoid fitting cannot achieve the calibration effect, and the calculated parameters are also wrong. But our algorithm can still calibrate in this case, the RMS (the root mean square of distance from each measurement to the ideal sphere) is reduced from 71.1165uT to 11.7660uT, The three pictures on the right in Figure 2 shows the calibration effect in three cases. They illustrate the same conclusion: our algorithm enables a convenient magnetometer calibration.

6.2. Accuracy and speed experiment

We use the same method in 6.1 to obtain *mag-raw*, calibration parameters and *sphere-ideal*. Then input *mag-raw* of different time periods into the three algorithms to get the calculation parameters.

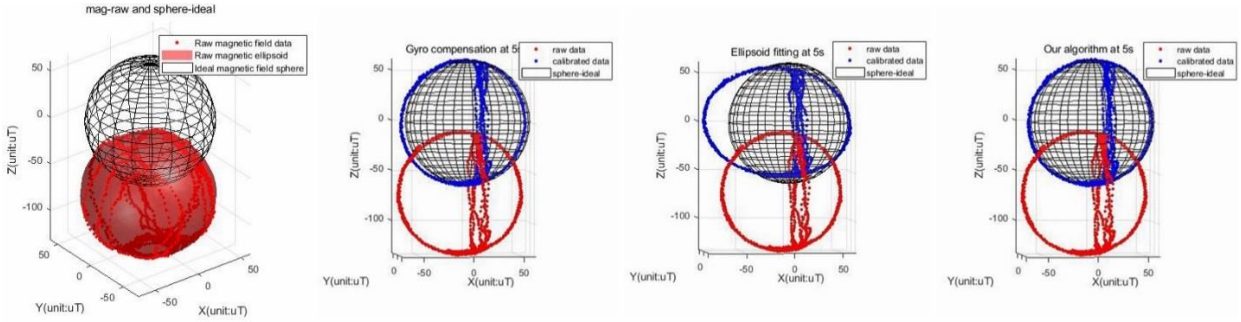

Figure 3. Raw magnetic field data, ideal magnetic field sphere and the effect of three algorithms at 5s

The left picture in Figure 3 shows the original magnetic field data and the ideal magnetic field sphere. It can be found that the original magnetic field data cannot be well distributed on the ideal sphere surface due to the soft and hard iron interference. From the three pictures on the right in Figure 3, we can find that the calibrated data of our algorithm fits better than the other two, indicating the accuracy of our algorithm is higher. The parameters calculated by each algorithm are shown in table 2.

Table 2. Parameters obtained by each algorithm at 5s

	mag-raw's parameters	*mag-cal-elli*'s parameters	*mag-cal-gyro*'s parameters	*mag-cal-our*'s parameters
W	$\begin{bmatrix} 0.9880 & -0.0373 & 0.0009 \\ -0.0373 & 1.0344 & -0.0154 \\ 0.0009 & -0.0154 & 0.9800 \end{bmatrix}$	$\begin{bmatrix} 0.8098 & -0.0336 & 0.0319 \\ -0.0336 & 1.1384 & -0.0196 \\ 0.0319 & -0.0196 & 1.0877 \end{bmatrix}$	$\begin{bmatrix} 0.9863 & -0.0614 & -0.0052 \\ -0.0614 & 1.0314 & -0.0224 \\ -0.0052 & -0.0224 & 0.9830 \end{bmatrix}$	$\begin{bmatrix} 0.9933 & -0.0618 & -0.0047 \\ -0.0618 & 1.0275 & -0.0187 \\ -0.0047 & -0.0187 & 0.9797 \end{bmatrix}$
V	$\begin{bmatrix} -8.3567 \\ -11.7763 \\ -70.5351 \end{bmatrix}^{T}$	$\begin{bmatrix} 1.0382 \\ -12.3140 \\ -71.0914 \end{bmatrix}^{T}$	$\begin{bmatrix} -4.4250 \\ -11.0506 \\ -69.9746 \end{bmatrix}^{T}$	$\begin{bmatrix} -7.1447 \\ -10.9669 \\ -70.0546 \end{bmatrix}^{T}$
B	62.32uT	58.75uT	62.11uT	62.43uT

From this experiment, it can be found that the algorithm proposed in this paper takes less time to complete the calibration than the ellipsoid fitting, and the calibration accuracy is better than the gyro-only compensation. Our algorithm enables fast, high precision real-time calibration.

6.3. Stability experiment

The purpose of this experiment was to test the stability of the gyro-only compensation algorithm and our algorithm. We first fully rotate the LMPS-B2 to let the algorithms have enough data to adjust the parameters. Then the sensor is placed in static for 10 minutes.

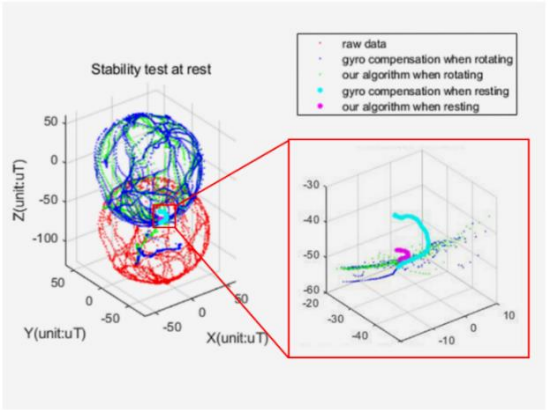

Figure 4. Calibrated data from both algorithms

As shown in Figure 4 after the sensor is stationary, the magnetometer data should be stable at some point, but in the gyro-only compensation algorithm, the data will gradually drift due to the drift of the gyroscope. But our algorithm fuses data of accelerometer and gyroscope, because of the long-term stability of the accelerometer, the output magnetometer data drift is reduced. The linear distance from the first data to each subsequent data at rest of our algorithm are 4.12uT, and gyro-only compensation algorithm is 11.10uT. Our algorithm can significantly reduce the degree of drift compared to the gyro-only compensation algorithm, indicating that it has strong stability.

In order to test the impact of different drifts on the two algorithms, we first remove the inherent drift of the gyroscope in the LMPS-B2, and then manually added different levels of drift on the gyroscope's three-axis data. Finally, these data are brought into the algorithm to compare the drift distance of the magnetometer data.

Table 3. Comparison of stability under artificial drift

Artificial drift	0.1dps	0.2dps	0.3dps	0.4dps	0.5dps
Drift distance of our algorithm	1.90uT	2.82uT	3.85uT	4.50uT	5.47uT
Drift distance of gyro-only compensation	3.81uT	8.55uT	13.38uT	17.44uT	21.10uT
Rate of two distance	49.8%	33.0%	28.8%	25.8%	25.9%

Table 5 shows that when the magnetometer is stationary, our algorithm can better make the gyroscope data at a certain point. indicating that our algorithm enables better stability of the magnetometer calibration.

From this experiment, we can find that our algorithm uses the improved complementary filtering to fuse the acceleration and gyroscope data, so it can reduce the drift of the gyroscope, which achieves stable magnetometer calibration.

7. Conclusion

The magnetometer is highly susceptible to interference from surrounding ferromagnetic materials. This paper first improves the traditional complementary filtering to eliminate the influence of linear acceleration during motion, then uses it fuses the accelerometer and gyroscope data to make more accurate prediction of the magnetometer data, and then an Extended Kalman Filtering are used to implement magnetometer calibration. Finally, a convenient, accurate and stable real-time magnetometer calibration algorithm is realized. It has a wide range of functions in consumer electronics, vehicle inertial navigation systems and military.

References

[1] LIU G X, SHI L F. An overview about development of indoor navigation and positioning technology [J]. *Journal of Navigation and Positioning*, 2018,6(2): 7-14.
[2] PAN X F, MU H, HU X P. A Survey of Autonomous Navigation Technology for Individual Solder [J]. *Navigation Positioning and Timing* ,2018,5(1): 1-11.
[3] PEI L, LIU D H, QIAN J C. A Survey of Indoor Positioning Technology and Application [J]. *Navigation Positioning and Timing*, 2017,4(3): 1-10.
[4] WANG L. Research on Key Technologies of Combined Heading System [D]. *Northwestern Polytechnical University*, 2007.
[5] ZHOU N B, WANG Y B, WANG Q. A brief review of geomagnetic navigation technology [J]. *Journal of Navigation and Positioning*, 2018,6(2): 15-19.
[6] YANG B F, FAN B Y, XU J M, et al. Research on Error Compensation in Geomagnetic Field Measurement Based on Least Squares [J]. *Journal of Air Force Engineering University (Natural Science Edition)*, 2017,18(6): 34-39.
[7] ZHOU J, GE Z L, SHI G G, et al. Development and Key Technologies of Geomagnetic Navigation [J]. *Journal of Astronautics*, 2008,29(5): 1467-1472.

[8] QIN G, GUNA X Y, LI W S. Compensation method of magnetic field error of three-dimensional vector based on ellipsoid compensation [J]. *Electronic Measurement Technology*, 2018,41(2): 34-39.
[9] Wu Y, Pei L. Gyroscope Calibration via Magnetometer[J]. *IEEE Sensors Journal*, 2017, 17(16): 5269-5275.
[10] Kok M, Schon T B. Magnetometer Calibration Using Inertial Sensors[J]. *IEEE Sensors Journal*, 2016, 16(14): 5679-5689.
[11] K. Han, H. Han, Z. Wang and F. Xu, "Extended Kalman Filter-Based Gyroscope-Aided Magnetometer Calibration for Consumer Electronic Devices," in *IEEE Sensors Journal*, vol. 17, no. 1, pp. 63-71.
[12] Euston M, Coote P W, Mahony R E, et al. A complementary filter for attitude estimation of a fixed-wing UAV[C]. *intelligent robots and systems*, 2008: 340-345.
[13] Wu Y, Zou D, Liu P, et al. Dynamic Magnetometer Calibration and Alignment to Inertial Sensors by Kalman Filtering[J]. *IEEE Transactions on Control Systems and Technology*, 2018, 26(2): 716-723.
[14] ZHU J L, WANG X Q, WU P L, et al. Three-dimensional magnetic compass error compensation algorithm based on ellipsoid surface fitting [J]. *Journal of Chinese Inertial Technology*, 2012,20(5): 562-566.
[15] Valenti R, Dryanovski I, Xiao J, et al. Keeping a Good Attitude: A Quaternion-Based Orientation Filter for IMUs and MARGs[J]. *Sensors*, 2015, 15(8): 19302-19330.